Sustainable Energy & Fuels
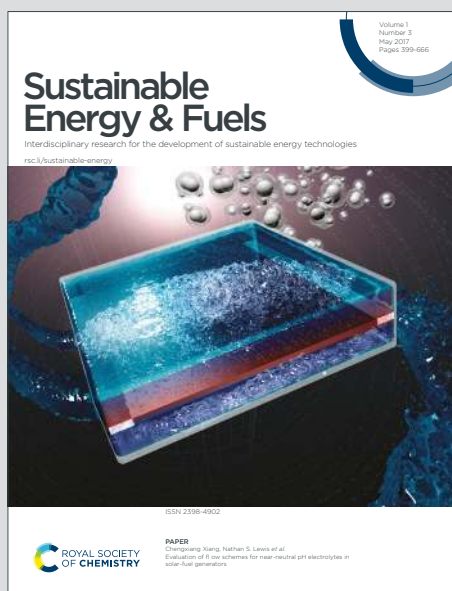
Interdisciplinary research for the development of sustainable energy technologies

Accepted Manuscript

Volume 1
Number 3
May 2017
Pages 399-666

Sustainable Energy & Fuels

Interdisciplinary research for the development of sustainable energy technologies

rsc.li/sustainable-energy

ISSN 2398-4902

ROYAL SOCIETY OF CHEMISTRY

PAPER
Chengxiang Xiang, Nathan S. Lewis et al.
Evaluation of fl ow schemes for near-neutral pH electrolytes in solar-fuel generators

This is an Accepted Manuscript, which has been through the Royal Society of Chemistry peer review process and has been accepted for publication.

Accepted Manuscripts are published online shortly after acceptance, before technical editing, formatting and proof reading. Using this free service, authors can make their results available to the community, in citable form, before we publish the edited article. We will replace this Accepted Manuscript with the edited and formatted Advance Article as soon as it is available.

You can find more information about Accepted Manuscripts in the Information for Authors.

Please note that technical editing may introduce minor changes to the text and/or graphics, which may alter content. The journal's standard Terms & Conditions and the Ethical guidelines still apply. In no event shall the Royal Society of Chemistry be held responsible for any errors or omissions in this Accepted Manuscript or any consequences arising from the use of any information it contains.

ROYAL SOCIETY OF CHEMISTRY

rsc.li/sustainable-energy

ARTICLE

Interface Engineering of Mesoporous Triphasic Cobalt-Copper Phosphides as Active Electrocatalysts for Overall Water Splitting

Ali Saad,[a] Zhixing Cheng,[a,b] Hangjia Shen,[a,b] Haichuan Guo,[a,b] John Paul Attfield,[c*] Tiju Thomas,[d*] Minghui Yang[a,b*]

Efficient electrocatalysts for water splitting are essential for viable generation of highly purified hydrogen. Hence there is a need to develop robust catalysts to eliminate barriers associated with sluggish kinetics associated with both anodic oxygen and cathodic hydrogen evolution reactions. Herein, we report a two-step approach nanocasting-solid phase phosphorization approach to generate ordered mesoporous triphasic phosphides CoP@Cu$_2$P-Cu$_3$P. We show that it is a highly efficient bifunctional electrocatalyst useful for overall water splitting. The mesoporous triphasic CoP@Cu$_2$P-Cu$_3$P only requires a low overpotential of 255 mV and 188 mV to achieve 10 mA cm^{-2} for oxygen and hydrogen evolution reactions, respectively. The combination of mesoporous pores (~5.6 nm) with very thin walls (~3.7 nm) and conductive networks in triphasic CoP@Cu$_2$P-Cu$_3$P enable rapid rate of electron transfer and mass transfer. In addition, when CoP@Cu$_2$P-Cu$_3$P is used to fabricate symmetric electrodes, the high surface area mesoporous structure and synergetic effects between phases together contributes to a low cell voltage of 1.54 V to drive a current density 10 mA cm^{-2}. This performance is superior to noble-metal-based Pt/C-IrO$_2$/C. This work provides a new approach for the facile design and application of multiphase phosphides as highly active bifunctional and stable electrocatalysts for water-alkali electrolyzers.

Introduction

Water electrocatalysis is an electrochemical energy conversion solution of choice since it offers a clean, sustainable route to high-purity hydrogen production.[1] Electrochemical water splitting can be divided into two half reactions, the oxygen evolution reaction (OER, $2H_2O \rightarrow O_2 + 4H^+ + 4e^-$) and hydrogen evolution reaction (HER, $2H^+ + 2e^- \rightarrow H_2$). Due to their low overpotentials and greater activity, precious metal Ru, Ir,[2] and Pt [3],[4] are considered as benchmark anodic OER and cathodic HER catalysts, respectively. Nevertheless, the high cost and scarcity of these noble metal-based electrocatalysts severely limits their widespread use.[5] In recent years, a variety of transition metal catalysts have been reported in order to further the possibility of commercializing fuel cells and electrolyzers. The compounds used include transition metal oxides,[5] metal nitrides,[6] metal phosphides,[7] and sulfides.[8] However, most of these materials, especially in their single phase are still far away from offering the desired combination of high activity and stability in the any given electrolyte.[9]

Due to their significant abundance, intrinsic metallic behavior, high conductivity and excellent stability a variety of transition metal phosphides (TMPs) such as FeP,[10] NiP,[11] Co$_2$P [12] and MoP, [13],[14] have been developed as alternatives to Pt-based catalysts. Thus far, cobalt phosphides-based catalysts have been found to be relevant for oxygen evolution electrocatalysis because of their promising activity at reasonable overpotentials. This is especially true for materials such as Co-oxo-hydroxyl phosphates,[15] Co-Pi/CoP [16] and mixed-metal oxyphosphides.[17] However, their catalytic performance ought to be improved further, to render them practically relevant.

One approach towards further improvement of cobalt phosphides would be through the synergistic effects caused by the atomic and electric coupling of bimetallic TMPs. For example, Jin et al. reported the synthesis of self-supported Cu$_3$P–Ni$_2$P hexagonal nanosheet arrays on commercially available nickel foam. These bimetallic phosphides show a low overpotential of 103 mV at a current density of 10 mA cm^{-2}, which is 47 and 100 mV less than that for Ni$_2$P/NF and Cu$_3$P/NF toward HER.[18] Another approach involves the formation of porous structured TMPs with large surface areas and numerous active sites. This offers a means to promote reaction kinetics and facilitate mass transport which is advantageous for catalytic reactions. Typical synthesis methods for TMPs are solid phase reaction,[12] vapor-phase deposition [19] and electrodeposition.[20] However, there remain technical difficulties and fundamental challenges in the control of features associated with ordered nanostructured materials using these approaches.

a. Ningbo Institute of Materials Technology and Engineering Chinese Academy of Sciences Ningbo 315201, China. E-mail: myang@nimte.ac.cn
b. Center of Materials Science and Optoelectronics Engineering, University of Chinese Academy of Sciences, Beijing 100049, China.
c. Centre for Science at Extreme Conditions and School of Chemistry University of Edinburgh Kings Buildings, West Mains Road, Edinburgh EH9 3JJ, UK E-mail: j.p.attfield@ed.ac.uk
d. Department of Metallurgical and Materials Engineering Microstructure Indian Institute of Technology Madras Adyar Chennai 600036, Tamil Nadu, India. E-mail: tijuthomas@iitm.ac.in
† Footnotes relating to the title and/or authors should appear here.
Electronic Supplementary Information (ESI) available: [details of any supplementary information available should be included here]. See DOI: 10.1039/x0xx00000x

ARTICLE

In this context of the need for decorated three dimensional (3D) phosphides with large surface areas, sophisticated architectures and high-density active sites; we report an interface engineering of ordered triphasic phosphides system - CoP@Cu$_2$P-Cu$_3$P - for electrochemical water splitting in alkaline medium. Mesoporous triphasic CoP@Cu$_2$P-Cu$_3$P is prepared in two steps; starting with nanocasting of mesoporous Co-Cu oxides from a KIT-6 hard silica template. This is followed by phosphorization using sodium hypophosphite. The as-synthesized 3D mesoporous CoP@Cu$_2$P-Cu$_3$P offers numerous active sites and efficient charge transfer which also accounts for enhanced electrocatalytic performance. At a current density of 10 mA cm^{-2}, as-developed triphasic electrocatalyst CoP@Cu$_2$P-Cu$_3$P produced excellent OER activity in an alkaline medium at overpotential of only 255 mV. On the other hand, a rather nominal overpotential of 188 mV is required for HER to attain the same current density. Consequently, an efficient two-electrode water electrolyzer has subsequently been fabricated. It required a cell voltage of only 1.54 V to reach a current density of 10 mA cm^{-2}. It also offered sufficient stability under continuous operation for 24 h.

Results and discussion

Ordered mesoporous triphasic cobalt-copper phosphides are fabricated via a nanocasting process as shown in Figure. S1 in Supporting Information. Briefly, cobalt and copper nitrates precursors are impregnated into the pores of large surface area mesoporous KIT-6 (Figure. S2). This is followed by silica etching using NaOH solution. Finally, Co$_2$CuO$_4$ mesoporous spinel oxide is converted to CoP@Cu$_2$P-Cu$_3$P via a gas-solid phosphidation reaction in a ceramic crucible at 360 °C for 3 h at a ramping rate of 4 °C min^{-1} in phosphine atmosphere (Figure. 1a and Figure. S3). Following the same procedure, for comparison, we also prepare mesoporous CoP and Cu$_3$P single phases from their corresponding nanotemplated mesoporous parent Co$_3$O$_4$ and CuO oxides (Synthetic details are given in experimental section in the Supporting Information).

Figure. S4 shows powder diffraction patterns of mesoporous CoP, Cu$_3$P and mesoporous triphasic CoP@Cu$_2$P-Cu$_3$P. The diffractogram of CoP shows peaks that could be indexed to (011), (111), (211), (202) and (301) plane reflections in the orthorhombic phase of CoP (JCPDS No. 00-029-0497).[21] As for Cu$_3$P, the diffraction peaks at 36.30, 39.31, 41.97, 45.05, 46.37, 47.53 and 66.67 correspond to the reflections of (112), (202), (211), (300), (113), (212) and (223) planes, respectively. These are consistent with hexagonal Cu$_3$P phase (JCPDS No.71-2261).[22] After phosphorization is completed, using the mesoporous spinel oxide Co$_2$CuO$_4$, the corresponding samples are labelled as CoP@Cu$_2$P-Cu$_3$P. This sample shows a mixture of three phases; an orthorhombic phase of CoP, hexagonal Cu$_3$P phase and monoclinic Cu$_2$Pphase. Moreover, by varying the cobalt/copper ratio different samples of CoP@Cu$_2$P-Cu$_3$P with different controllable phase composition and distribution are obtained (Figure. S5). The Rietveld refinement of the observed XRD patterns confirms the resultant crystalline phases without

any detectable impurity (Figure. S6a, 6b and 6c). The actual ratio of each phase is determined and the results are listed in Figure. S6d.

The mesostructure formation of Co$_2$CuO$_4$ and CoP@Cu$_2$P-Cu$_3$P is evidenced by the low-angle XRD (Figure. 1b). Characteristic diffraction peaks appear at 2θ=0.77° and 2θ=1.15°. These correspond to the (211) and (220) reflections on a 3D Ia3d cubic arrangement.[23] This is also supported by the BET analysis carried out at 77 K (Figure. S7). Both samples show Type IV isotherms with hysteresis loops that are typical for mesoporous materials.[24] The template-free mesostructured materials have BET surface area of 155.2 and 146.05 m^{2}g^{-1} with pore size distributions ranging from 4 to 6 nm, for Co$_2$CuO$_4$ and CoP@Cu$_2$P-Cu$_3$P, respectively.

The structure and morphology of as-prepared mesoporous materials are further investigated using TEM and SEM. Typical transmission electron microscopy (TEM) images of mesoporous Co$_2$CuO$_4$ (Figure. 1c) show a highly ordered porous structure arranged in a three-dimensional manner. The pores are connected and retain the symmetry of the parent silica KIT-6.[21] Uniform and well-ordered mesopores arranged in three-dimensional structure are observed in the TEM images of both CoP and Cu$_3$P (Figure. S8b and S8c) with diameter of pores and thickness of approximately ~5 to 7 nm and ~4.5 nm, respectively. After phosphidation reaction over Co$_2$CuO$_4$, the resultant mesoporous triphasic CoP@Cu$_2$P-Cu$_3$P (Figure. 1d) retains a regular mesoporous structure with an average pore size 5.57 nm and thickness of 3.7 nm (Figure. S9). Obviously, such large accessible pore networks and well-defined structure are particularly favorable for the full exposure of electrocatalytically active centers and for mass transfer necessary for electrocatalysts.[25]

The high-resolution TEM image of CoP@Cu$_2$P-Cu$_3$P interface is collected for further structural information. As shown in Figure. 1e, a wide range of well-crystallized walls exist around the small mesopores. This is clearly seen from the integrated crystal lattice pattern and three distinct resolved lattice fringes. The distinctive lattice fringes with an interplane spacing of 0.28 nm is in accordance with the (102) reflection for orthorhombic CoP. The second one with an interplane spacing of 0.22 nm can be attributed to (112) plane of hexagonal phase Cu$_3$P. On the other hand, the third one has an interplane spacing of 0.22 nm, which can be assigned to the (100) plane of monoclinic Cu$_2$P. This is in good agreement with the XRD, and offers proof of the formation of CoP, Cu$_2$P and Cu$_3$P nanocrystallites.

Inset Figure. 1e shows the selected area electron diffraction (SAED) pattern of mesoporous triphasic CoP@Cu$_2$P-Cu$_3$P. The multiple diffraction circles can be indexed to the (-112) crystal plane of monoclinic Cu$_2$P, the (011) and (112) crystal planes of the orthorhombic CoP [26,27] as well as the (300) and (113) planes of the hexagonal phase Cu$_3$P.[22] All of these clearly demonstrate the high crystallinity of mesoporous triphasic CoP@Cu$_2$P-Cu$_3$P. Low-magnification SEM shown in Figure. 1f is used to characterize the shape and the surface morphology. As-prepared mesoporous bimetallic CoP@Cu$_2$P-Cu$_3$P particles exhibit spherical shape and particle sizes in the range of 200–300 nm. The mesopores are distributed throughout the

interior of nanoparticles. The HAADF-STEM image and corresponding EDS elemental mapping (Figure. 1g) confirm the presence Co (purple), Cu (green) and P (red) and obviously show homogeneous and uniform distribution across the selected

area. The molar ratio of Co/Cu in CoP@Cu$_2$P-Cu$_3$P, determined from the EDX spectrum (Figure. S10), is around 1.92, which is close to the expected Co/Cu ratio of 2.
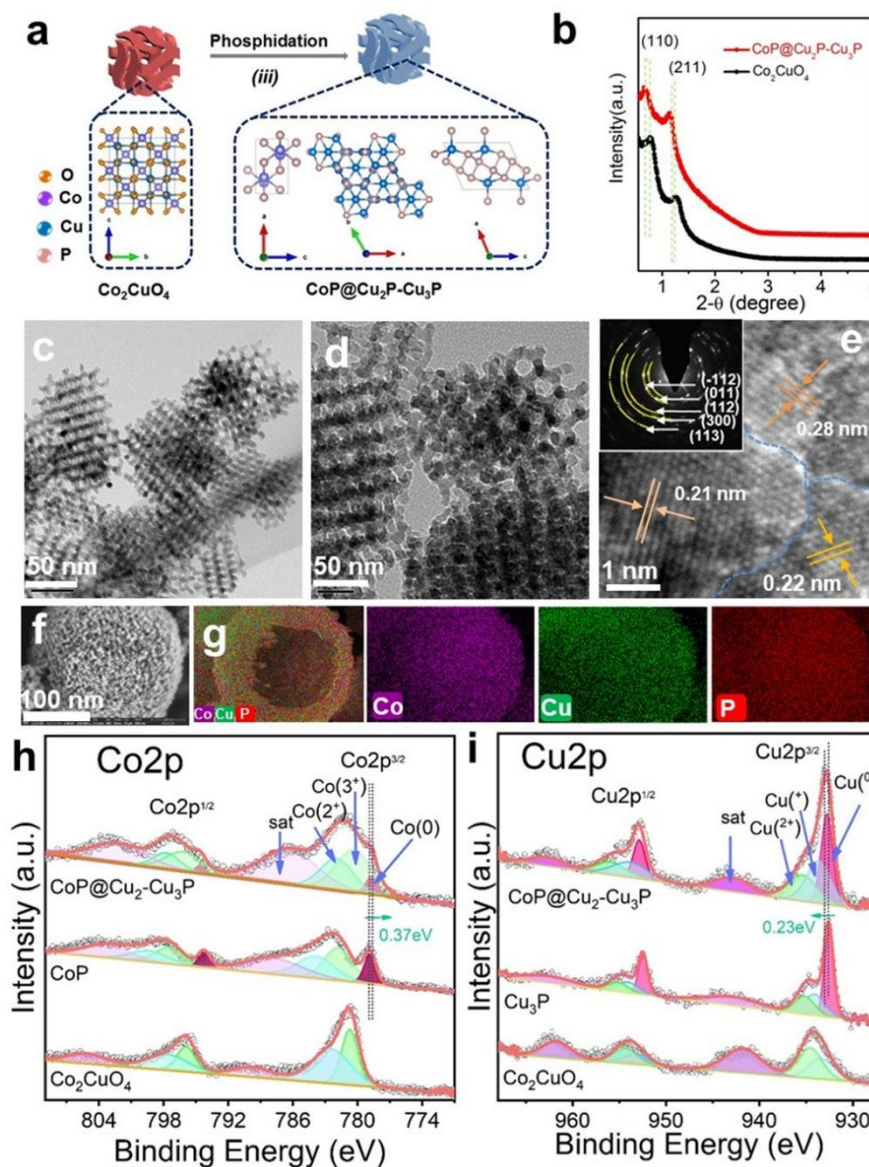
Fig. 1 (a) Gas-solid phosphidation reaction conversion of Co$_2$CuO$_4$ mesoporous spinel oxide to CoP@Cu$_2$P-Cu$_3$P. (b) Low-angle powder XRD patterns of silica-free mesoporous Co$_2$CuO$_4$ and CoP@Cu$_2$P-Cu$_3$P. TEM images of highly ordered mesoporous: (c) Co$_2$CuO$_4$, (d) CoP@Cu$_2$P-Cu$_3$P. (e) HRTEM of mesoporous triphasic phosphides CoP@Cu$_2$P-Cu$_3$P (inset indicates formation of CoP, Cu$_2$P and Cu$_3$P phases at the interface with their d-spacing and the SAED patterns of CoP@Cu$_2$P-Cu$_3$P showing reflections from three phases simultaneously. (f) Low-magnification SEM images of typical morphology for CoP@Cu$_2$P-Cu$_3$P (g) EDS elemental mapping of CoP@Cu$_2$P-Cu$_3$P. High-resolution XPS spectra (h) Co2p and (i) Cu 2p for Co$_2$CuO$_4$, CoP, Cu$_3$Pand CoP@Cu$_2$P-Cu$_3$P.

The elemental compositions and chemical states of as-synthesized mesoporous Co$_2$CuO$_4$ and their corresponding mesoporous triphasic CoP@Cu$_2$P-Cu$_3$P are characterized using X-ray photoelectron spectroscopy (XPS). The XPS survey spectrum of Co$_2$CuO$_4$ notably revealed the presence of peaks corresponding to Co 2p, Cu 2p, and O 1s and C 1s that exist in the sample (Figure. S11a). Phosphorization for

mesoporous triphasic system is demonstrated by the concomitant appearance of the P 2p feature centered at 133.3 eV.[28] This is consistent with the result of its EDS elemental mapping. The high-resolution XPS spectra of Co 2p (Figure. 1h) for mesoporous Co$_2$CuO$_4$, CP and CoP@Cu$_2$P-Cu$_3$P display binding energies of Co 2p$_{3/2}$ and Co 2p$_{1/2}$ separated by a spin-orbit splitting of 15.3 eV. This is

confirmed by the presence of mixed oxidation states of Co (II) and Co (III).[29] The fitting of the Co 2p for mesoporous Co_2CuO_4 shows two spin-orbit doublets that can be attributed to the Co^{2+} and Co^{3+} species. The associated shake-up satellite peaks (indicated by "Sat") are assigned to Co^{2+} and Co^{3+} components.[30] After phosphorization, $CoP@Cu_2P-Cu_3P$ shows an additional component with low binding energy located at about 777.9 eV in Co 2p3/2 and 793.1 eV in Co 2p1/2. This is a typical feature of the metallic state (Co^0) in CoP, indicating the formation of CoP, consistent with previous reports.[31,32]
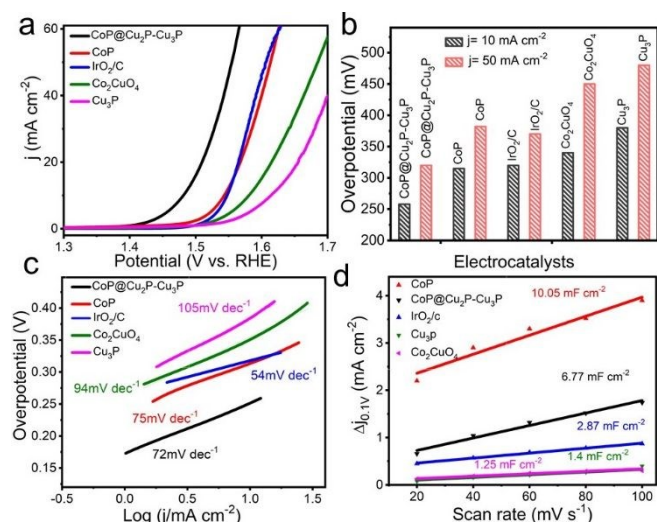

Fig. 2 (a) OER polarization curves in O_2-saturated 1 M KOH (sweep rate: 5 mV s^{-1}; rotation speed: 1600 rpm). (b) Required overpotentials to achieve 10 and 50 mA cm^{-2} current density. (c) Tafel plots with the corresponding Tafel slopes. (d) Capacitive current density at 0.10 V as a function of the scan rate for mesoporous Co_2CuO_4, CoP, Cu_3P, $CoP@Cu_2P-Cu_3P$ and benchmark catalyst IrO_2/C.

The profile of the Cu 2p spectra (Figure 1i) shows the two doublets Cu $2p_{3/2}$ at 933.8 eV and Cu $2p_{1/2}$ at 954.5 eV with a spin-orbit separation of 20.7eV. Cu $2p_{3/2}$ peak can be deconvolved into three peaks: 932.5, 934.4 and 941.4 eV; these are identified as a typical feature of Cu^+, Cu^{2+} and associated satellite peak.[33] After phosphorization, as is the case for Co 2p, an additional component with low binding energy appears which is located at 932.5 eV corresponding metallic state (Cu^0) in Cu-P. This too indicates the successful formation of copper phosphide in mesoporous triphasic $CoP@Cu_2P-Cu_3P$ system. The binding energy corresponding to Co (^{0}) in the Co2p spectrum of $CoP@Cu_2P-Cu_3P$ negatively shifted 0.37 eV compared with pure CoP, whereas Cu2p reveals a upward shift of 0.23 eV for Cu (^{0}) in $CoP@Cu_2P-Cu_3P$ when compared to the phase pure phosphides Cu_3P. This result reveals that the electronic structures are adjusted due to the interfacial charge transfer caused by different arrangement of electron clouds for CoP, Cu_3P and Cu_2P in the ternary phosphide system.[34] Which can optimize adsorption of intermediates.[35] Figure. S11b display the deconvoluted graph of P 2p spectra, which indicates that the electronic configuration of the mesoporous $CoP@Cu_2P-Cu_3P$ is resolved into two components which are not visible in the

parent spinel oxide template. The peaks centered at 129.5 eV are typical of metal-phosphide bonds (Cu-Co-P), while the second peak at 133.8 eV can correspond to the oxidized phosphorus in the form of PO_4^{3-}.[23] Hence, XPS results further confirm complete phosphorization and the formation of the mesoporous triphasic $CoP@Cu_2P-Cu_3P$ system.

Given the well-defined mesoporous structures, and the large accessible pore networks present in triphasic $CoP@Cu_2P-Cu_3P$ systems, the electrocatalytic activities of mesoporous electrocatalysts toward OER are investigated. This is done in 1 M KOH using linear sweep voltammetry (LSV) with standard three-electrode system. The counter electrode wire is the platinum net, and the Ag/AgCl (in a saturated KCl solution) electrode is used as the reference electrode. A glassy carbon electrode coated with electrocatalysts serves as working electrode to catalyse OER process at a scan rate of 5 mV s^{-1} with the same loading density of ~ 0.203 mg cm^{-2}. The commercial IrO_2/C is systematically examined, since it serves as a suitable benchmark catalyst. All the measured potentials for OER polarization curves are calibrated based on reversible hydrogen electrode (RHE) (see the Experimental Methods in the Supporting Information for details).

Figure. 2a shows the polarization curve with iR compensation of mesoporous Co_2CuO_4, CoP, Cu_3P, and $CoP@Cu2P-Cu_3P$ and benchmark IrO_2/C catalysts. The mesoporous triphasic Co-Cu (2:1) phosphides has an onset potential at 1 mA cm^{-2} of 1.43 V (vs RHE), which is much lesser than the value for single phase CoP (1.50 V), Cu_3P (1.55 V) and the Co-Cu spinel oxide (1.56 V). Moreover, among the surveyed catalysts, triphasic $CoP@Cu_2P-Cu_3P$ exhibits a significantly lower overpotential (η) and it offers much greater current density (j) values (Figure. 2b). For instance, $CoP@Cu_2P-Cu_3P$ can achieve overpotential ($η_{10}$) of 255 mV at a geometric current density of 10 mA cm^{-2}. In contrast, CoP, IrO_2/C, Co_2CuO_4 and Cu_3P require significantly larger overpotentials (η) of 313, 319, 340 and 379 mV to offer the same current density (10 mA cm^{-2}). Similar results are also observed for overpotentials at higher current densities.

The overpotential $η_{50}$ value at 50 mA cm^{-2} is found to be 318 mV for $CoP@Cu_2P-Cu_3P$, which is 63, 52, 131, and 161 mV, all of which are less than that of the CoP, IrO_2/C, Co_2CuO_4 and Cu_3P, respectively. These overpotentials are comparable to those of other state-of-the-art OER catalysts, such as $(Co_{0.52}Fe_{0.48})_2P$,[36] $Co_3(OH)_2(HPO_4)_2/NF$,[37] and much smaller than those reported ones for bimetallic Co-Cu based catalysts such as $CuCo_2S_4$,[38] $CuCo_2Se_4$,[39] and CuCoP-NC-700.[40] This indicates that as-synthesized mesoporous triphasic $CoP@Cu_2P-Cu_3P$ is a promising OER catalyst (See Table S1).

Furthermore, the Tafel slope which is an important kinetic parameter to explain the high catalytic performance is obtained from the extrapolation of the linear region of a plot of overpotential vs log j (Figure. 2c).[41] The mesoporous triphasic $CoP@Cu_2P-Cu_3P$ possesses a Tafel slope of 72 mV dec^{-1} is superior to the value for CoP, Co_2CuO_4 spinel oxide and Cu_3P were (75 mV dec^{-1} V), (94 mV dec^{-1}) and (105 mV dec^{-1}), respectively. This implies that very minimal overpotential is required to enhance current density for OER

on CoP@Cu$_2$P-Cu$_3$P. Additionally, the interconnected porous channels on the mesoporous triphasic phosphides facilitate the release of the generated gas leading to more favorable electrocatalytic kinetics.

To further explain the reasons for the excellent OER activity, the electrochemical surface areas (ECSAs) of as-prepared catalysts are evaluated under different operating conditions by capacitance measurements via cyclic voltammograms as shown in Figure. S13. The charging currents are collected at different scan rates (20, 40, 60, 80, and 100 mV s^{-1}) in the potential window of 0.04 to 0.12 V. The double-layer capacitance values are calculated from the linear fit of current density change at 0.10 V as a function of scan rate (Figure. 2d). The mesoporous triphasic CoP@Cu$_2$P-Cu$_3$P has a capacitance C$_{dl}$ of 6.77 mF cm^{-2} while the value for mesoporous CoP, Cu$_3$P, Co$_2$CuO$_4$ spinel oxide and IrO$_2$/C are 10.05, 1.4, 1.25 and 3.5 mF cm^{-2}, respectively. This reflects a high electrochemical surface area, and consequently a high surface roughness associated with the triphasic CoP@Cu$_2$P-Cu$_3$P system.

In order to exclude the influence of surface area on the intrinsic activity, the LSV current density is normalized to the electrochemical surface areas (Figure. S14a and S14b). The ECSA can be calculated from the C$_{dl}$ according to the ratio: ESCA= C$_{dl}$/C$_s$, where C$_s$ is the specific capacitance, and is chosen to be C$_s$ = 0.040 mF·cm^{-2} in 1 M KOH based on reported values [42] (See Table S2). The mesoporous triphasic CoP@Cu$_2$P-Cu$_3$P possesses an ECSA of 169.25 cm^2 with an intrinsic catalyst activity (0.596 mA cm^{-2} ESCA at η = 370 mV) which is superior to the single cobalt phosphide (0.159 mA cm^{-2} ESCA), copper phosphide (0.21 mA cm^{-2} ESCA), Co-Cu oxides (0.493 mA cm^{-2} ESCA) and benchmark IrO$_2$/C (0.524 mA cm^{-2} ESCA). These results exhibit excellent intrinsic activity, indicating more active sites generated in the associated mesoporous triphasic CoP@Cu$_2$P-Cu$_3$P toward OER activity. This contributes to the superior OER activity of CoP@Cu$_2$P-Cu$_3$P when compared to other electrocatalysts. In addition, electrochemical impedance spectroscopy (EIS) is performed to evaluate the electrode kinetics. As shown in Figure 14c, the EIS plots reveal that the CoP@Cu$_2$P-Cu$_3$P catalyst possesses much smaller semicircle diameter, highlighting the higher conductivity.

For nanostructured catalysts, durability is vital due to the enhanced atom mobility on nanoscale surfaces. Normalized chronopotentiometric j-t curves are measured by employing mesoporous triphasic CoP@Cu$_2$P-Cu$_3$P catalyst at 1.5 V vs RHE (Figure. S14d). It is found that the long-term stability of the sample is excellent. The working potential required to hold the current density raises by only 5.5% after 10 h of continuous operation.

In addition to the oxygen evolution activities of the mesoporous triphasic CoP@Cu$_2$P-Cu$_3$P, performance towards HER is also assessed at an equivalent loading mass in 1 M KOH solution. Figure. 3a shows the linear sweep voltammetry (LSV) curves of CoP@Cu$_2$P-Cu$_3$P and the reference sample electrocatalysts include Co$_2$CuO$_4$, CoP, Cu$_3$P and benchmark 20% Pt/C. As expected, the Pt activity is far superior when compared to the transition metal

phosphides. Triphasic CoP@Cu$_2$P-Cu$_3$P exhibits a remarkably small overpotential of 188 mV at a current density of 10 mA cm^{-2}, which is small when compared to that of prepared mesoporous catalysts CoP (330 mV), Cu$_3$P (349 mV) and Co$_2$CuO$_4$ (480 mV) (Figure. 3b). Another point worth noting is that at such a high current density (i.e. at 50 mA cm^{-2}), the mesoporous CoP@Cu$_2$P-Cu$_3$P catalyst only requires an overpotential of 251 mV, which is rather small when compared to mesoporous phosphide single phases CoP (410) and Cu$_3$P (462 mV). This suggests a positive effect associated with the formation of a triphasic system: CoP, Cu$_2$P and Cu$_3$P. Phosphor (P) draws electrons and captures protons from Co and Cu due to its higher electronegativity. This facilitates desorption of hydrogen and acting as sites for H$_2$ dissociation therefore enhances HER performance,[43] as revealed by density functional theoretical calculations reported.[44] This is also consistent with reports on other bimetallic alloys Cu$_3$P– Ni$_2$P,[18] Ni/Co/Fe phosphosulfide,[45] and ternary Co$_{1-x}$Ni$_x$P$_3$.[46] Corresponding Tafel plots indicate that the CoP@Cu$_2$P-Cu$_3$P electrode possess a Tafel slope of ~89 mV dec^{-1}, which is larger than the 39 mV dec^{-1} for the benchmark Pt/C system (Figure. 3c). This suggests a Volmer-Tafel mechanism.[46] However, CoP@Cu$_2$P-Cu$_3$P exhibits the smallest Tafel slope when compared to the values - 92, 152 and 131 mV dec^{-1}, which are observed for single phase CoP, Cu$_3$P and Co$_2$CuO$_4$, respectively. This indicates efficient rapid kinetic activities and electron transfer due to a synergistic interaction between different metallic phosphide sites.
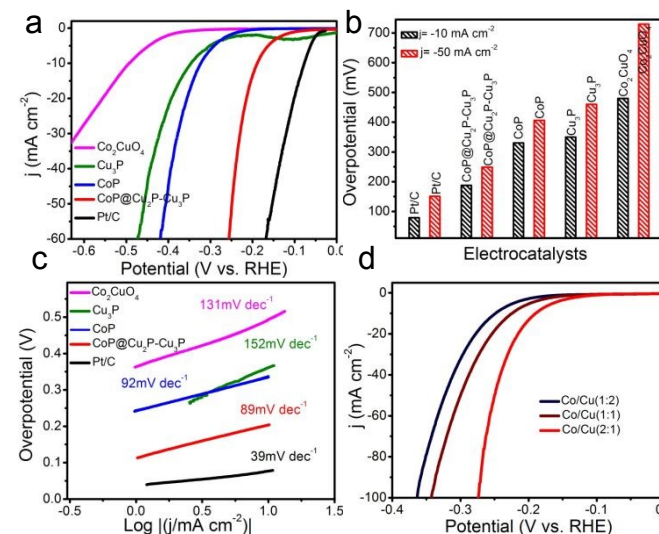

Fig. 3 (a) HER polarization curves in O$_2$-saturated 1 M KOH (sweep rate: 5 mV s^{-1}; rotation speed: 1500 rpm) Co$_2$CuO$_4$, CoP, Cu$_3$P, CoP@Cu$_2$P-Cu$_3$P and benchmark catalyst Pt/C. (b) Overpotentials required for j = 10 and 50 mA cm^{-2}. (c) The corresponding Tafel plot. (d) LSVs showing the HER activity of CoP@Cu$_2$P-Cu$_3$P with Co: Cu (2:1, 1:1, 2:1) ratio.

Stability tests are also conducted which show no obvious change in the overpotential of 200 mV after continuous 1000 cyclic voltammetry cycles (Figure. S15a). Furthermore, we carry out durability testing with chronoamperometric measurements (j-t). As depicted in Figure. S15b, the

mesoporous CoP@Cu$_2$P-Cu$_3$P shows no obvious loss in current density for 10 h, revealing its superior stability.

Moreover, to emphasize the importance of Co/Cu ratio in the mesoporous triphasic phosphides, Figure. 3d shows the polarization curves of CoP@Cu$_2$P-Cu$_3$P junction with different Co/Cu ratios in 1.0 M KOH. It is found that with the decrease of copper phosphide amount in mesostructured triphasic phosphides, there is an obvious improvement in the HER catalysis. The mesoporous triphasic CoP@Cu$_2$P-Cu$_3$P with Co/Cu (2:1) ratio has the highest HER performance. These results suggest that Cu doping is beneficial for improving the HER catalytic performance of cobalt phosphide. This is due to the following factors (i) low doping of metals phosphides by copper phosphide has already proven to be a good way to improve in the catalytic action [9, 47]. (ii) Higher electron transfer conductivity of copper phosphides contributes to superior HER activity of CoP@Cu$_2$P-Cu$_3$P. CoP single phase shows a lower overpotential toward HER as compared to Cu$_3$P. This means that higher amounts of cobalt when compared to copper will be beneficial towards improvement the catalytic performance in the CoP@Cu$_2$P-Cu$_3$P catalyst [47].

Inspired by the impressive bifunctional catalytic activities and durability for both HER and OER, the overall water splitting activity in 1 M KOH solution is evaluated. As shown in Figure. 4a a single electrolyzer equipped with a two-symmetric electrode modified by the as-synthesized mesostructured CoP@Cu$_2$P-Cu$_3$P

as cathode and anode has been built. The catalyst is loaded on Ni foam at a mass loading of 1 mg cm^{-2}. During the electrolysis process, a large number of bubbles can be clearly seen from both the cathode (H$_2$) and anode (O$_2$) (Figure. S16). As shown in Figure. 4b, the CoP@Cu$_2$P-Cu$_3$P LSV curves without iR correction for overall water splitting performance. As synthetized triphasic CoP@Cu$_2$P-Cu$_3$P requires a relatively low cell voltage of 1.54 V to achieve a stable current density of 10 mA cm^{-2}. Long-term stability tests of the mesoporous triphasic CoP@Cu$_2$P-Cu$_3$P under the overall water splitting conditions with a two-step chronopotentiometry response is shown in Figure. 4c. Importantly, it is obvious that the potential is found to be quite stable without any visible voltage elevation of the current density for both 10 and 100 cm^{-2} current density trace. In comparison with noble-metal-based Pt/C-IrO$_2$/C, mesoporous triphasic CoP@Cu$_2$P-Cu$_3$P electrolyzer show marginally better performance and better durability (Figure. S17a and 17b). This cell voltage is also much smaller than other mesoporous triphasic CoP@Cu$_2$P-Cu$_3$P with different Co/Cu ratio (Figure. S18). As a bifunctional electrocatalyst, the performance of mesoporous triphasic CoP@Cu$_2$P-Cu$_3$P overall water splitting surpasses many previously reported state-of-the-art alkaline media electrocatalysts (a detailed comparison in Figure. 4d and Table S3). This indicates the advantage afforded by the combination of distinguished architecture, composition, and synergetic effects of the active center of phosphides phases.
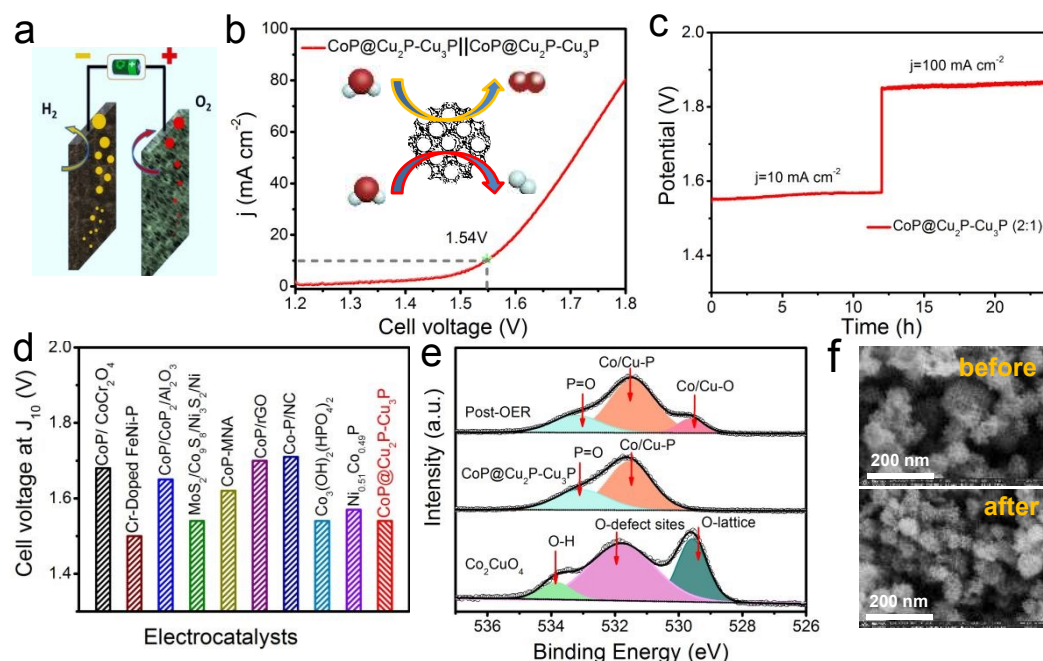

Fig. 4 (a) Schematic diagram of overall water splitting. (b) LSV polarization curve without iR compensation for mesoporous CoP@Cu$_2$P-Cu$_3$P symmetric electrodes in 1 M KOH for overall water splitting. (c) Durability of overall water splitting for a current density trace of 10–100 cm^{-2} for CoP@Cu$_2$P-Cu$_3$P. (d) Comparison of overall water-splitting performance of CoP@Cu$_2$P-Cu$_3$P symmetric electrodes in 1 M KOH couple with recently reported Co-based electrocatalysts in alkaline electrolyte. (e) High-resolution XPS spectra O1s for Co$_2$CuO$_4$, CoP@Cu$_2$P-Cu$_3$P before and after water-splitting process. (f) Low-magnification SEM images of typical morphology for CoP@Cu$_2$P-Cu$_3$P before and after water-splitting process.

ARTICLE

Furthermore, in order to examine the structural durability, we have considered the characterizations of the mesostructured CoP@Cu$_2$P-Cu$_3$P electrolyzer after electrochemical measurement. Due to the strong oxidation condition, the metal ions trapped in porous catalyst can effectively be converted into MOOH particles by partial surface oxidation of the TMP. [48,49] As shown in Figure. 4e, oxygen high resolution in Co$_2$CuO$_4$, CoP@Cu$_2$P-Cu$_3$P before and after water splitting. The O1s spectra in Co$_2$CuO$_4$ can be deconvolved to three contributions assigned to spinel oxide lattice, oxygen from the defect sites, and oxygen from physical and chemisorbed water. After phosphorization, CoP@Cu$_2$P-Cu$_3$P spectrum displays two components at 531.5 and 533.06 eV attributed to Co/Cu-O-P and P-O,[32] respectively. In addition, to the above-mentioned peaks CoP@Cu$_2$P-Cu$_3$P, after water splitting stability test, we observe a third peak with low binding energy at 529.5 eV. This peak can be related to the oxidized cobalt and copper metallic species which is regarded as the active site to enhance the catalytic performance.[48] We also investigate the possible morphology changes of as prepared triphasic CoP@Cu$_2$P-Cu$_3$P catalyst before and after electrochemical measurement. Figure. 4f shows a nanospherical structure-like with particle sizes in the range of 100–300 nm over the whole material. Hence the morphology remains largely unchanged with bicontinuous distribution after the stability test without any obvious change confirming the excellent structural stability against collapsing pores or channels due to oxygen bubbling during the electrocatalysis process.[50]

Based on the above, mesostructured triphasic phosphide is shown to have well-defined 3D structure with abundant exposed active sites enable efficient electrolyte diffusion and rapid gas bubble escape.[51] In addition, it also offers the synergistic effect between metal elements in phosphide phases (CoP, Cu$_2$P and Cu$_3$P) enabling the tuning of the electronic structure and modulation on the absorption energy of the reaction intermediates.[52] Due to good electrical conductivity of copper phosphides that decreases the resistance of the catalytic system, the introduction of copper phosphides into CoP leads to improve the intrinsic electrochemical properties of the hybrid catalyst and thus impressively contribute to the high OER activity and excellent stability. The oxygen high resolution XPS, performed after electrochemical measurement suggests the formation of surface metal (oxy)hydroxide species which are known to be robustly active sites for OER.[53] In keeping with existing reports, it appears plausible that here too phosphorization of metal modifies the binding energy between metal and hydrogen, leading to the optimal Gibbs free energy for hydrogen evolution.[54]

Conclusions

In conclusion, a mesostructured triphasic CoP@Cu$_2$P-Cu$_3$P system with abundant exposed active sites and highly accessible surfaces has been synthesized using a nanocasting process followed by a gas-solid phosphidation reaction. As a result, the mesoporous CoP@Cu$_2$P-Cu$_3$P shows outstanding OER and HER behaviors in an alkaline solution with very low overpotential of 255 mV and 188 mV to yield 10 mA cm^{-2}, respectively. The mesoporous triphasic system evidently offers superior performance to single phase phosphides (CoP and Cu$_3$P). The enhanced catalytic performance derives from its intrinsic activity as well as conductivity. Thus, through synergistic effects arising out of structure, interconnectivity of pores, and catalytic behavior, mesoporous CoP@Cu$_2$P-Cu$_3$P offers champion activities. When assessed in an alkaline water electrolyzer, with CoP@Cu$_2$P-Cu$_3$P as both the anode and cathode, operation is possible at a low cell voltage of 1.54 V with 24 h durability. Morphological retention, and electrocatalytic stability was also observed. We anticipate this work to push existing boundaries for rational design and facile fabrication of highly active and noble-metal free catalysts for electrocatalysis.

Conflicts of interest

The authors declare no competing financial interests.

Acknowledgements

Notes and references

1   (a)I. Roger, M.A. Shipman, M.D. Symes, Nat. Rev. Chem. 2017, 1, 1-13. (b) X, Liu R, Guo K, Ni F, Xia C, Niu B, Wen J, Meng P, Wu J, Wu X, Wu L. Mai Adv. Mater 2020, 32, 2001136. (c) X. Liang, J. Xiao, W. Weng, W. Xiao, *Angew Chem Int Ed*. 2020. https://doi.org/10.1002/anie.202013257

2   Y. Yuan, S. Adimi, X. Guo, T. Thomas, Y. Zhu , H. Guo , G.S. Priyanga , P. Yoo, J.Wang , J. Chen , P. Liao, J. P. Attfield, M. Yang, Angew. Chem. Int. *Ed*. 2020, 59,18036-18041.

3   J.R. McKone, E.L. Warren, M.J. Bierman , S.W. Boettcher , B.S. Brunschwig , N.S. Lewis, H.B. Gray, Energy Environ. Sci. 2011, 4,3573-3583.

ARTICLE

Journal Name

4   (a) S. Ye, F. Luo, Q. Zhang, P. Zhang, T. Xu, Q. Wang, D. He, L. Guo, Y. Zhang, C. He, X. Ouyang, Energy Environ. Sci. 2019, 12, 1000-1007.(b) C. Huang, D. Wu, P. Qin, K. Ding, C. Pi, Q. Ruan, H. Song, B. Gao, H. Chen, P.K. Chu, *Nano Energy*, 2020, 104788.

5   (a) F. Song, L. Bai, A. Moysiadou, S. Lee, C. Hu, L. Liardet, X. Hu. J. Am. Chem. Soc.2018, 140, 7748-7759. (b) X. Xu, Y. Pan, Y. Zhong, R. Ran, Z. Shao, *Materials Horizons*, 2020. *7*, 2519-2565.

6   (a) K. Xu, P. Chen , X. Li, Y. Tong, H. Ding, X. Wu, W. Chu, Z. Peng, C. Wu ,Y. Xie, J.Am. Chem. Soc. 2015,137, 4119-4125. (b) Z. Wang, L. Xu, F. Huang, L. Qu, J. Li, K. A. Owusu, Z. Liu, Z. Lin, B. Xiang, X. Liu, K. Zhao, X. Liao, W. Yang, Y.B. Cheng, L. Mai, Adv. Energy Mater. 2019, 1900390

7   (a) J. Song, C. Zhu, B. Z. Xu, S. Fu, M. H. Engelhard, R. Ye, D. Du, S. P. Beckman, Y. Lin, Adv. Energy Mater. 2017, 7, 1601555. (b) L. Ji, J. Wang, X. Teng, T. J. Meyer, Z. Chen, ACS Catal. 2020, 10, 412–419.

8   Y. Guo, J. Tang, J. Henzie, B. Jiang, W. Xia, T. Chen, Y. Bando, Y.M. Kang, M.S.A. Hossain, Y. Sugahara, Y. Yamauchi. ACS nano.2020, 14, 4141-4152.

9   (a) L. Yan, B. Zhang, J. Zhu, S. Zhao, Y. Li, B. Zhang, J. Jiang, X. Ji, H. Zhang, P.K. Shen, J. Mater. Chem. A.2019, 7, 14271-14279.(b) X.Q. Cao, J. Zhou, S. Li, G.W. Qin, *Rare Metals*, *39*(2), 2020, 113-130.

10   X. Li, W. Liu, M. Zhang, Y. Zhong, Z. Weng, Y. Mi, Y. Zhou, M. Li, J.J. Cha, Z. Tang, H. Jiang, Nano Letters 2017;17:2057-2063.

11   E.J. Popczun, J.R. McKone, C.G. Read, A.J. Biacchi, A.M. Wiltrout, N.S. Lewis, R.E Schaak. J. Am. Chem. Soc 2013, 135, 9267-9270.

12   J.F. Callejas, C.G. Read, E.J. Popczun, J.M. McEnaney, R.E. Schaak, Chem. Mater.2015, 27, 3769-3774.

13   J. Yang, F. Zhang, X.Wang, D. He, G. Wu, Q. Yang, X. Hong, Y. Wu, Y. Li. Angew Chem Int Ed 2016, 55,12854-12858.

14   R. Ge, J. Huo, T. Liao, Y. Liu, M. Zhu, Y. Li, J. Zhang, W. Li, Appl. Catal. B Environ 2020, 260, 118196.

15   J. Chang, Y. Xiao, M. Xiao, J. Ge, C. Liu, W. Xing. ACS Catal. 2015, 5, 6874-6878.

16   Y.P. Zhu, Y.P. Liu, T.Z. Ren, Z.Y. Yuan, Adv. Funct. Mater 2015, 25,7337-7347.

17   B.Y. Guan, L.Yu, X.W.Lou, Angew Chem Int Ed, 2017, 56, 2386-2389.

18   X. Jin, J. Li, Y. Cui, X. Liu, X. Zhang, J. Yao, B. Liu, Inorg. Chem. 2019, 58, 11630-11635.

19   M. Asnavandi, B. H. R. Suryanto, W. Yang, X. Bo, C. Zhao, ACS Sustainable Chem. Eng. 2018, 6, 2866–2871.

20   F. Yu, H. Zhou, Y. Huang, J. Sun, F. Qin, J. Bao, W.A. Goddard, S. Chen, Z. Ren , Nat. Commun, 2018, 9, 1-9.

21   A. Saad, H. Shen, Z. Cheng, Q. Ju, H. Guo, M. Munir, A. Turak, J. Wang, M. Yang, ACS Appl. Energy Mater, 2020, 3, 1684-1693.

22   S. Wei, K. Qi, Z. Jin, J. Cao, W. Zheng, H. Chen, X. Cui, ACS omega 2016,1,1367-1373.

23   A. Saad, H. Shen, Z. Cheng, R. Arbi, B. Guo, L.S. Hui, K. Liang, S. Liu, J. P. Attfield, A. Turak, J. Wang, M. Yang, Nano Micro Lett 2020, 12,1-3.

24   K. S. Sing, D. H. Everett, R. A. W. Haul, L. Moscou, R. A. Pierotti, J. Rouquerol, T. Siemieniewska, Pure Appl. Chem 1982, 54, 2201.

25   K. Liu, F. Wang, P. He, T.A. Shifa, Z. Wang, Z. Cheng, X. Zhan, J. He, Adv. Energy Mater, 2018, 8, 1703290.

26   L. Ji, H. Zheng, Y. Wei, Y. Fang, J. Du, T. Wang, S. Wang, Sustain. Energy Fuels, 2020, 4 , 1616-1620.

27   Z. Pu, Q. Liu, P. Jiang, A. M. Asiri, A. Obaid, X. Sun, Chem. Mater. 2014, 26, 15, 4326-4329

28   H. Zhang, X. Li, A. Hähnel, V. Naumann, C. Lin, S. Azimi, S.L. Schweizer, A.W. Maijenburg, R.B. Adv. Funct. Mater.2018, 2,1706847.

29   A. Amri, X. Duan, C.Y. Yin, Z.T. Jiang, M.M Rahman, T. Pryor, Appl. Surf. Sc.2013, 275, 127-135.

30   P. Li, W. Sun, Q. Yu, P. Yang, J. Qiao, Z. Wang, D. Rooney, K. Sun, Solid State Ion. 2016; 289: 17-22.

31   J. Kibsgaard, C. Tsai, K. Chan, J.D. Benck, J.K. Nørskov, F. Abild-Pedersen, T.F. Jaramillo, Energy Environ. Sci.2015, 8, 3022-3029.

32   A.P. Grosvenor, S.D. Wik, R.G. Cavell, A. Mar, Inorg. Chem. 2005, 44,8988-8998.

33   H.S. Jadhav, S.M. Pawar, A.H. Jadhav, G.M. Thorat, J.G. Seo, Sci. Rep.2016, 6, 31120.

34   H. Huang, H. Jung, H. Jun, D.Y. Woo, J.W. Han, J. Lee, Chemical Engineering Journal, 405.126977.

35   R. Boppella, J. Tan, W. Yang, J. Moon, Adv. Funct. Mater, 2019, 29, 1807976.

36   Y. Tan, H. Wang, P. Liu, Y. Shen, C. Cheng, A. Hirata, T. Fujita, Z. Tang, M. Chen, Energy Environ. Sci. 2016, 9, 2257-2261.

37   P.W. Menezes, C. Panda, C. Walter, M. Schwarze, M. Driess, Adv. Funct. Mater. 2019, 29, 1808632.

38   M. Chauhan, K.P. Reddy, C.S. Gopinath, S. Deka, ACS Catal 2017, 7, 5871-5879.

39   X. Cao, J.E. Medvedeva, M. Nath, ACS Applied Energy Materials 2020, 3, 3092-3103.

40   H. Zhang, Z. Yang, X. Wang, S. Yan, T. Zhou, C. Zhang, S.G. Telfer, S. Liu, Nanoscale 2019, 11,17384-17395.

41   D.T. Tran, H.T. Le, N.H. Kim, J.H. Lee , Appl. Catal. B Environ 2019, 253, 235-245.

42   Y. Zhang, L. Gao, E.J.M. Hensen, J.P. Hofmann, ACS Energy Lett. 2018, 3, 1360−1365.

43   A. Chunduri, S. Gupta, O. Bapat, A. Bhide, R. Fernandes, M. K. Patel, V. Bambole A. Miotello, N. Patel, Appl. Catal. B 2019, 259, 118051.

44   J. Joo, T. Kim, J. Lee, S.I. Choi, K. Lee, Adv. Mater. 2019,31,1806682.

45   M. Yao, H. Hu, B. Sun, N. Wang, W. Hu, S. Komarneni, Small 2019, 15, 1905201.

46 (a) Q. Fu, T. Wu, G. Fu,T. Gao, J. Han, T. Yao,Y. Zhang,W. Zhong, X. Wang, B. Song , ACS Energy Lett 2018, 3, 1744-1752. (b) M. Wang, Y. Tuo, X. Li, Q. Hua, F. Du, L. Jiang, ACS Sustain. Chem. Eng. 2019, 7, 12419-12427.

47   X., Ma, Y., Chang, Z. Zhang, J., Tang, J. Mater. Chem. A, 2018, *6*, 2100-2106.

48   L. Yang H. Liu H. Shen Y. Huang S. Wang L. Zheng D. Cao, Adv. Funct. Mater. 2020, 30, 1909889.

49   M.W. Kanan, D.G. Nocera, Science 2008, 321,1072-1075.

50   M. Yu, G.H. Moon, R.G. Castillo, S. DeBeer, C. Weidenthaler, H. Tüysüz, Angew. Chem. Int. Ed 2020 , 59, 16544-16552

51   L. Yu, J. Zhang, Y. Dang, J. He, Z. Tobin, P. Kerns, Y. Dou, Y. Jiang, Y. He, S.L. Suib, ACS Catal. 2019, 9, 6919−6928

52   Q. Liang, L. Zhong, C. Du, Y. Luo, J. Zhao, Y. Zheng, J. Xu, J. Ma, C. Liu, S. Li, Q. Yan, ACS Nano 2019, 13,7975-7984.

53   K. N. Dinh, P. Zheng, Z. Dai, Y. Zhang, R. Dangol, Y. Zheng, B. Li,Y. Zong, Q. Yan , Small 2018, 14 , 1703257.

54   (a) Y. Zhang, Q. Shao, S. Long, X. Huang, Nano Energy, 2018, 45, 448-455. (b) A. Saad, Z. Cheng X. Zhang, S. Liu, H. Shen, T. Thomas, J. Wang, M. Yang, *Advanced Materials Interfaces*, 2019. *6*, 1900960.

Interface Engineering of Mesoporous Triphasic Cobalt-Copper Phosphides as Active Electrocatalysts for Overall Water Splitting

Ali Saad,[a] Zhixing Cheng,[a,b] Hangjia Shen,[a,b] Haichuan Guo, [a,b] John Paul Attfield, [c*] Tiju Thomas, [d*] Minghui Yang [a,b*]

Ningbo Institute of Materials Technology and Engineering Chinese Academy of Sciences Ningbo 315201, China. E-mail: myang@nimte.ac.cn
Center of Materials Science and Optoelectronics Engineering, University of Chinese Academy of Sciences, Beijing 100049, China.
Centre for Science at Extreme Conditions and School of Chemistry University of Edinburgh Kings Buildings, West Mains Road, Edinburgh EH9 3JJ, UK E-mail: j.p.attfield@ed.ac.uk
Department of Metallurgical and Materials Engineering Microstructure Indian Institute of Technology Madras Adyar Chennai 600036, Tamil Nadu, India. E-mail: tijuthomas@iitm.ac.in
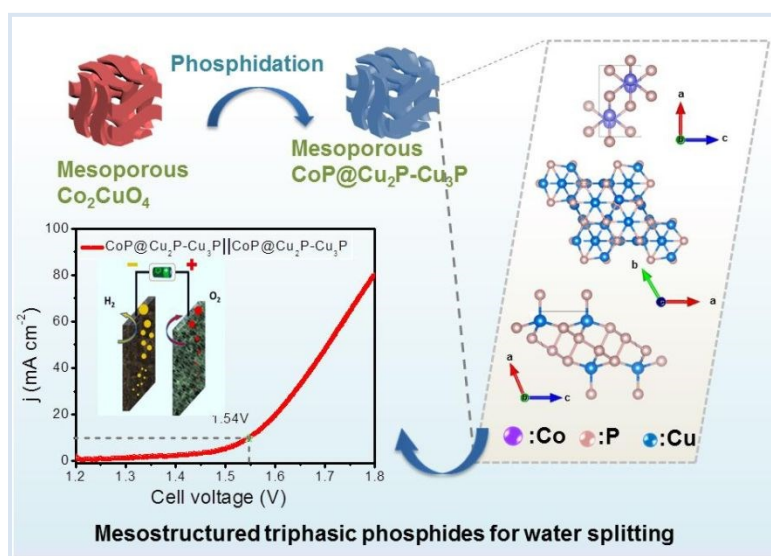
Three-dimensional (3-D) mesoporous triphasic cobalt-copper phosphides (CoP@Cu$_2$P-Cu$_3$P) with uniform shape and large surface area could be used as highly efficient bifunctional and stable electrocatalysts for water-alkali electrolyzers. These offer a lower cell voltage and more stability when compared to noble-metal-based Pt/C-IrO$_2$/C.